Journal of Alloys and Compounds 509 (2011) 758–763

Contents lists available at ScienceDirect

Journal of Alloys and Compounds

journal homepage: www.elsevier.com/locate/jallcom

Effects of Ag nanoshape and AgGa phase in Ag–Si nanostructure using 2-step etching process

Zhan-Shuo Hu [a], Fei-Yi Hung [b,*], Shoou-Jinn Chang [a,c,*], Kuan-Jen Chen [d], Wen-Long Wang [b], Sheng-Joue Young [d], Tse-Pu Chen [d]

[a] Institute of Electro-Optical Science and Engineering, Center for Micro/Nano Science and Technology, National Cheng Kung University, Tainan 701, Taiwan
[b] Institute of Nanotechnology and Microsystems Engineering, Center for Micro/Nano Science and Technology, National Cheng Kung University, Tainan 701, Taiwan
[c] Institute of Microelectronics & Department of Electrical Engineering, Center for Micr/Nano Science and Technology, National Cheng Kung University, Tainan 701, Taiwan
[d] Institute of Microelectronics, National Cheng Kung University, Tainan 701, Taiwan

ARTICLE INFO

Article history:
Received 18 February 2009
Received in revised form
14 September 2010
Accepted 17 September 2010
Available online 24 September 2010

Keywords:
Ag
Si
Etching
Nanostructure
Focus ion beam (FIB)

ABSTRACT

The etching scale was controled by the layball process and a focus ion beam (FIB) was used to investige the dry–wet etching (DWE) mechanism. Increasing the beam current of dry-etching raised the height of nano prominent structures, but deteriorated the interface of Ag/Si film, and even damaged the Ag film because of Ga^+ bombardment. Regardless of the Ag nanoshape deposition, the residual Ag films were doped with Ga^+ and were sensitive to DWE. After wet-etching, the nano hollow formed and the Ag films sunk. However, AgGa sidewall films formed by the concentration gradient and the oxidative potential and this increased the volume of microporous phases, resulting in a reduction in the depth. Also, 15–30 nm Ag nano-particles were able to enhance the DWE mechanism in the Ag/Si nanostructures.
© 2010 Elsevier B.V. All rights reserved.

1. Introduction

One dimension (1D) nanostructures have been attracting much interest following further improvement in miniaturization. Indeed, 1D nanostructures including the nanorod, the nanowire, the nanotube and so on have been fabricated for applications such as field effect transistors [1,2], field emission [3,4], light emitting devices and biotechnology with better characteristics [5]. Notably, due to advanced technology 1D Si nanostructures have also been applied to many areas, such as the vapor liquid solid method [6,7], thermal evaporation growth [8,9], related lithographic etching method [10,11] and chemical wet etching [12,13].

Recently, Fuhrmann et al. obtained arrays of aligned Si nanowires with tuneable diameter using patterned gold particles on a Si surface via nanosphere lithography [14]. Additionally, Peng et al. further combined nanosphere lithography and metal induced etching to fabricate aligned Si nanowire arrays [15]. Cheng Mu et al. produced Si nanotubes by using multistep template replication and chemical vapor deposition [16]. However, the above nanopatterns were structured using either dry-etching or wet-etching. In order to connect biotechnology [7] and semiconductor fabrication, the two step DWE (dry–wet etching, DWE) of Si nanohollow structure needs a development. Because the DWE is a new material process, its mechanism has still not been examined, and in particular the redox reaction and the effect of sidewalls. In this work, nanosphere lithography was done first, then the selective ion etching of Ag/Si film was performed using a focused ion beam (FIB). Finally, wet-etching finished the Ag/Si nanostructures. The DWE mechanism is closely related to the nanostructural characteristics and reliability of the Ag/Si thin film, so this study used Ag (30 nm)-Si film not only to analyze the effect of ion bombardment, but also to investigate the sinking mechanism for different Ag nanoshape depositions.

2. Experimental procedure

The monolayer 900 nm polystyrene (PS) suspension was dropped onto the glass substrate in air (Fig. 1(a)). Before usage, the aqueous suspension was diluted by deioned water at 1:2 wt.%, then was coated on the glass. The glass had good hydrophilicity which allowed the monolayer PS nanosphere to form uniformly at the hexagonal arrays. In the other way, the Ag thin film (30 nm) was sputtered on a p-Si surface. The sputter system was in a vacuum of 1.7×10^{-5} Torr and the reactive

* Corresponding authors. Tel.: +886 6 2757575x31395; fax: +886 6 2745885.
E-mail addresses: fyhung@mail.mse.ncku.edu.tw (F.-Y. Hung), changsj@mail.ncku.edu.tw (S.-J. Chang).

0925-8388/$ – see front matter © 2010 Elsevier B.V. All rights reserved.
doi:10.1016/j.jallcom.2010.09.076

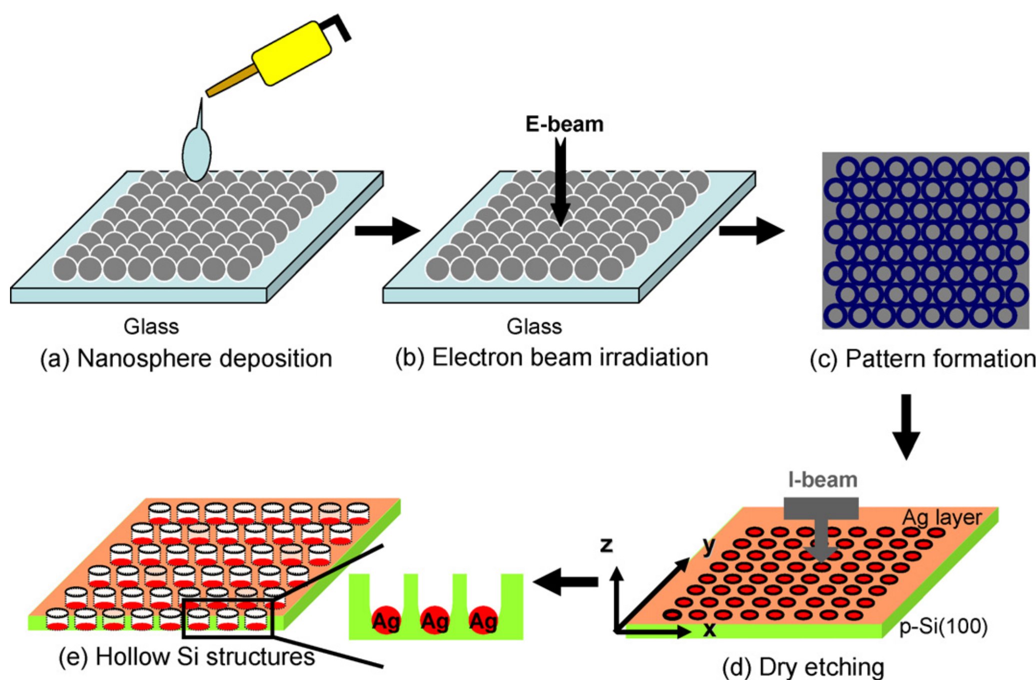

Fig. 1. Schematic diagram of fabrication of Si nano-tube using two-step etching. (a) a monolayer PS spheres on glass substrate, (b) SEM image of a monolayer PS spheres under electron beam irradiation, (c) the ring pattern formation, (d) the Ag nano-pattern on p-Si using dry etching of FIB, and (e) the formation of Si nanotube using wet etching.

gas was at a flow rate of 20 sccm (gas pressure was fixed at 15×10^{-3} Torr). The RF power was set at 60 W and the distance from the target to the sample surface was fixed at 3 in.

To obtain an image of the nanosphere array, glass with a nanosphere monolayer was used with the secondary electron signal, as shown in Fig. 1(b). Basically, the SEM images are based on the secondary electron signal and the aspect ratio of the object was controled. This study used the method of FIB selective etching pattern which can distinguish between dark zones and bright zones depending on the SEM image (Fig. 1(c)). The selective etching pattern was used to etch Ag/Si thin film through the FIB dry-etching and this is called the hexagonal-encircle ring pattern.

The formed hexagonal-encircle ring pattern was used to etch Ag/Si film to build the silver nanopattern as shown in Fig. 1(d). Finally, Ag patterned p-Si was given wet chemical etching to form the DWE nanostructures (Fig. 1(e)). The mixed solution included BOE (diluted by DI water 1:9 wt.%) and H_2O_2 (diluted by DI water 1:3 wt.%). BOE is composed of ammonium fluoride and hydrofluoric acid (BASF Electronic Materials Taiwan Co. Ltd.).

3. Results and discussion

3.1. Layball process and dry-etching mechanism

Fig. 2(a) shows the SEM image of the monolayer nanosphere and the corresponding hexagonal-encircle ring pattern which would be used for FIB dry-etching. The formation of the etching pattern was obtained from the SEM image of the nanospheres. Notably, related reports [17–19] used the monolayer nanospheres as the mask with lithography to etch surface structures (only one step). That even decreased the PS spheres to fabricate the nanopillars or nanowires. Here, the SEM images were divided into two zones (bright ring and dark circle) using an image analysis method (Fig. 2(b)). By the selective ion etching of FIB, either a ring or a

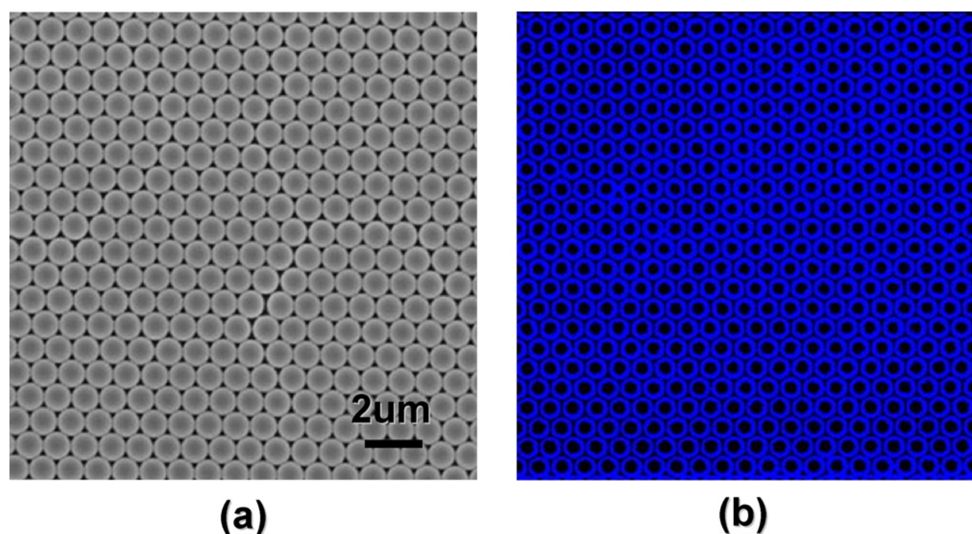

Fig. 2. (a) SEM image of monolayer nano-sphere and (b) real-time ring pattern formation using an image analysis method.

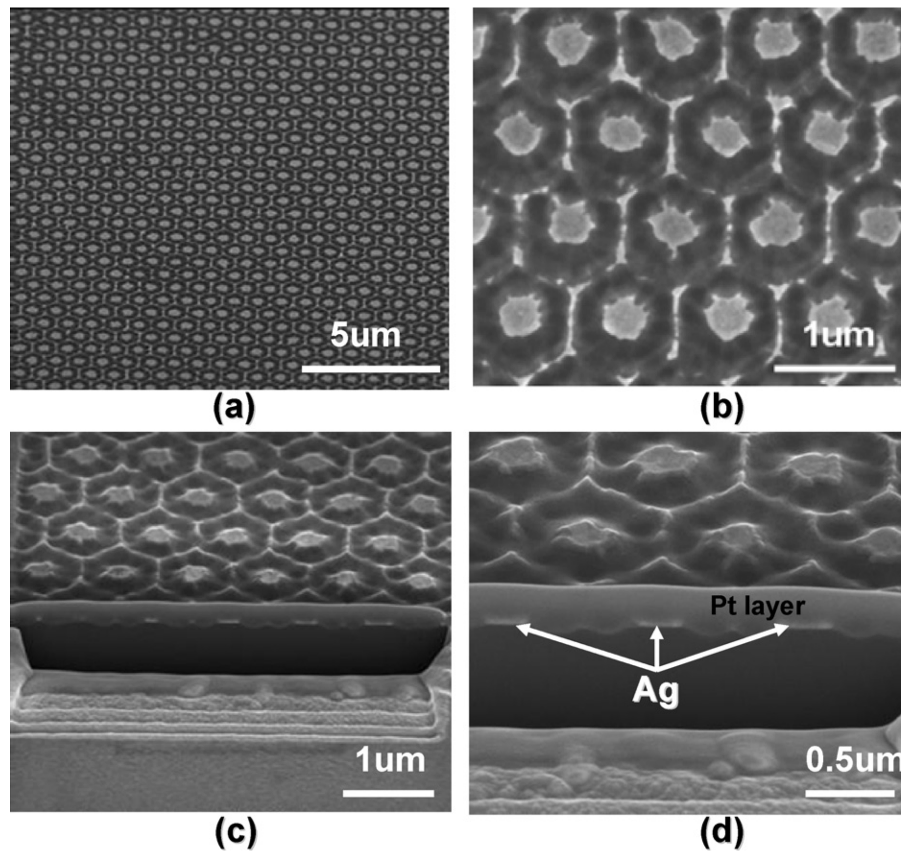

Fig. 3. SEM images of Si capped with 30 nm Ag thin film using dry etching: (a) Ag/Si nanostructure, (b) magnified image in (a), (c) cross-section observation, and (d) magnified image in (c).

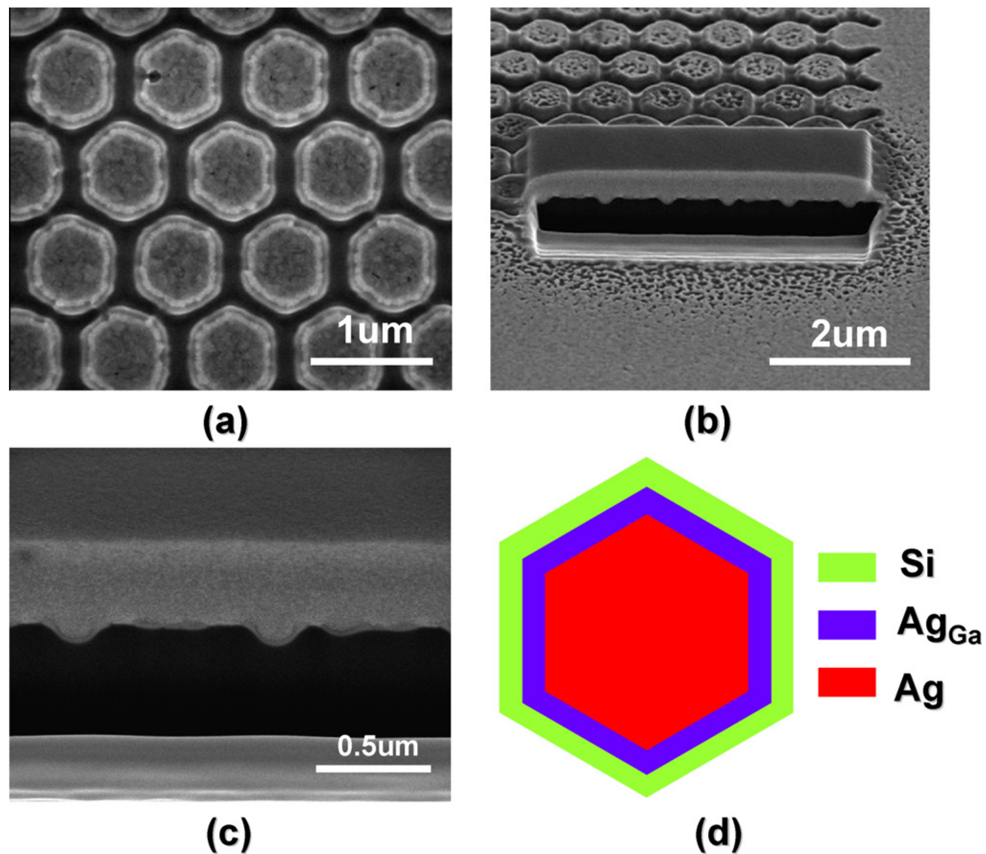

Fig. 4. FIB dry etching for a hexagonal pattern (a) top view, (b and c) cross-section image, and (d) schematic diagram of nanostructure in (a).

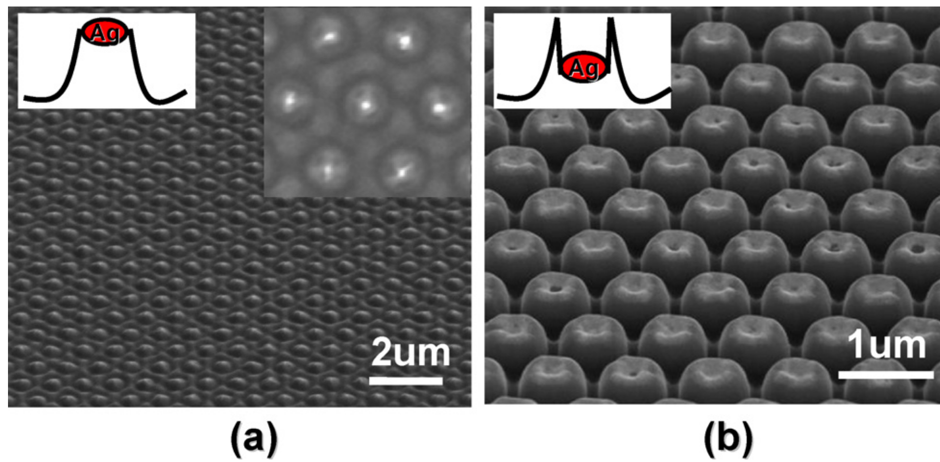

Fig. 5. Ag/Si nanostructure: (a) residual particle-like Ag on nano-rod, and (b) dot-hollow structure.

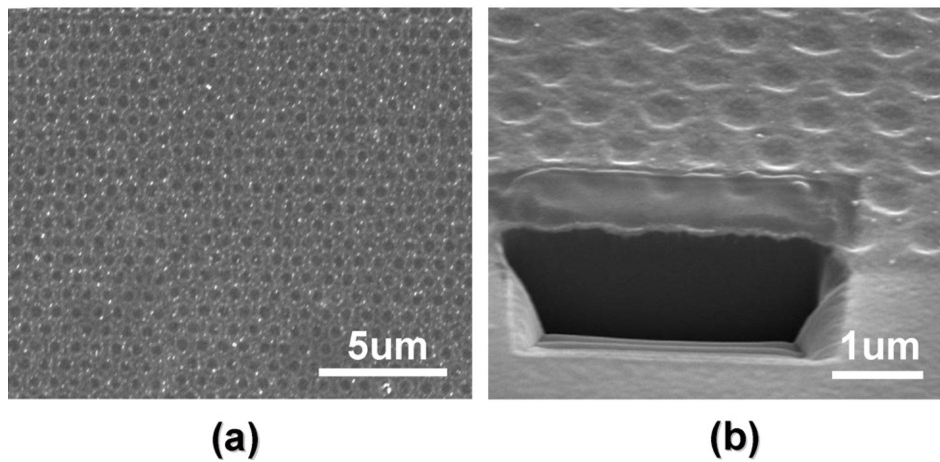

Fig. 6. Ag/Si nanostructures: (a) the nano-tube fabrication using the dry/wet etching and (b) the cross-section image.

circle was selected to etch the surface hexagonal-encircle ring pattern. In addition, the surface volume of a ring or a circle could been controled by the edge effect in electron microscopy using some parameters including threshold value, brightness and contrast. In Fig. 2(b), the blue color of the ring-pattern had been etched but that of the black circle had not been etched. After etching, the hexagonal-encircle ring pattern was obtained in the Ag/Si thin film.

Fig. 3 shows SEM images of the p-Si surface with a capping 30 nm silver layer and the cross-section of the specimen after ion dry-etching. We intentionally selected a smaller beam current of 50 pA to etch Ag/Si for 10 min in order to reduce ion damage to the side-

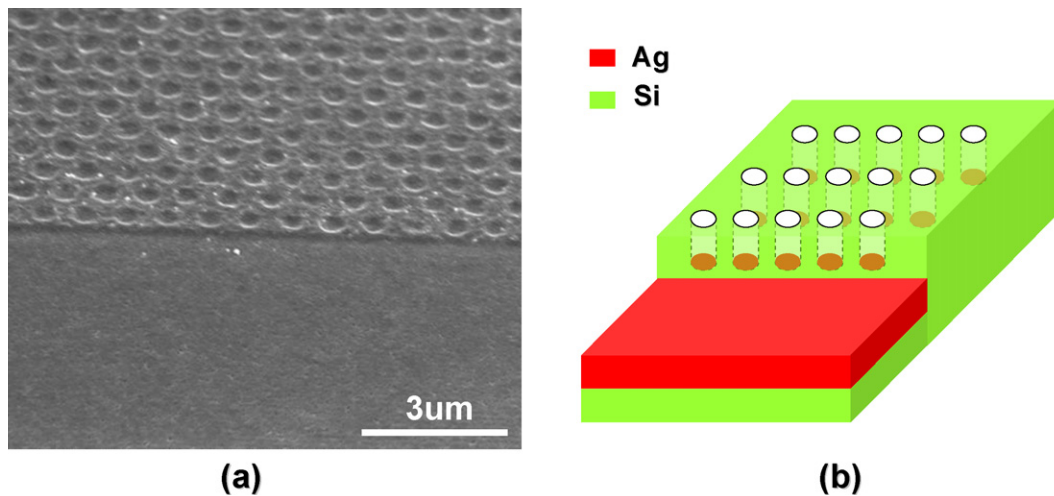

Fig. 7. (a) Wet etching surface characteristics of both Ag/Si nanotube and Si at tilted 52° view, and (b) the corresponding schematic diagram.

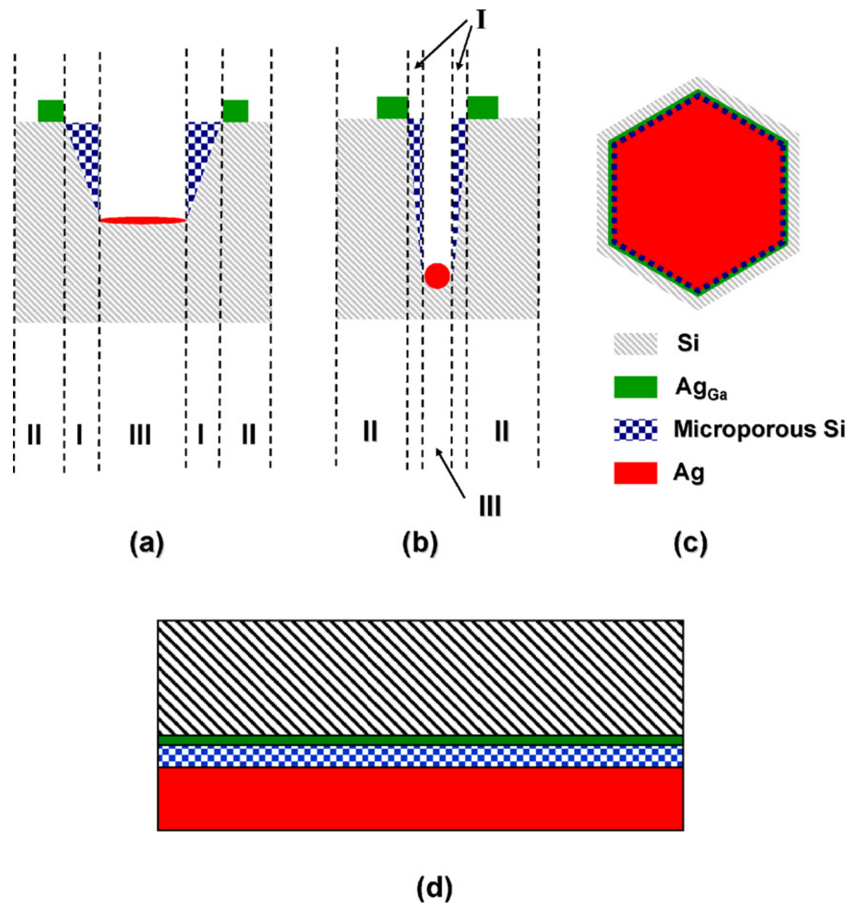

Fig. 8. Schematic diagram of etching mechanism for different Ag nano-shape: (a) Ag disk structure, (b) Ag particle, (c) nano-structure of top view after etching, and (d) schematic diagram of nanostructure on interface zone (Zone I: microporous Si).

wall of the etched area. The hexagonal-encircle ring pattern which appeared after FIB etching is shown in Fig. 3(a) and (b), and that was matched for the diameter of the original nanosphere. In fact, the ion dry-etching areas could be used as a stop layer for the next process (wet etching) because the etched areas had produced an Ag_{Ga} layer resulting from the ion bombarment [20].

Fig. 3(c) shows the cross-section image of the Ag/Si thin film after etching. The magnified image revealed a disk-like structure (Ag-disk: the diameter is 270 nm and the thickness is 30 nm) and the depth was 90 nm (Fig. 3 (d)). When the current of the ion beam was increased, the depth increased and the diameter of the Ag-disk decreased. The structure of the Ag-disk even became finer. When the first step dry-etching was finished, the surface structure was given the second step wet-etching to form the Ag/Si hollow nanostructure.

3.2. Nano-prominent structures

To increase the depth of the pattern and the thickness of the Ag_{Ga} layer, we used a the beam current of 100 pA (120 s) to perform dry etching and the surface characteristics are shown in Fig. 4(a). A discrete nanorod with an Ag-disk structure was observed and it looked like a honeycomb pattern. The difference between the hexagonal-encircle ring pattern and the honeycomb pattern is the surrounding bulge. In fact, when the brightness and contrast of Fig. 2 were increased, the etching structure transferred from a hexagonal-encircle ring pattern to a honeycomb pattern. Under the etching condition of the honeycomb pattern, the ion beam image (Fig. 4(a)) and the cross-section (Fig. 4(b) and (c)) revealed that the discrete Ag/Si nanorods possessed a multilayer structure. After EDS analysis, we were able to say that the top-structure of nano-prominent was Ag and the outside sidewall was Si. Due to the Ga^+ bombardment, the middle layer was AgGa (AgGa = Ag + Ga, Ga atoms solid in Ag matrix) sidewall film and the schematic diagram is shown in Fig. 4(d). It may be worth mentioning that the multilayer sidewall was able to assist the wet-etching process.

In addition, the honeycomb pattern was suitable for application of nanotube structure. In the first step dry-etching, the ion beam had Gaussian distribution to induce Ga doped Ag [21]. Because the strongest etching energy was in the central beam, the sidewall obtained more etching energy than the other zones (un-etched zones). This is why the sidewall showed an obvious doped effect. When increasing the ion beam current, some Ag films of nanorods still suffered from Ga^+ bombardment. Fig. 4 proves clearly that the top Ag film had been damaged. To avoid damage to the Ag films, the Ag nanoparticles (15 nm) were fabricated through FIB selective etching to perform the high energy dry-etching and the second step wet-etching.

3.3. Nano-hollow structures

In Fig. 5(a), residual Ag nanoparticles (15 nm) existed on the top of nanorods after FIB selective dry-etching. A second selective wet-etching was performed on this structure after completion of the first step dry-etching using a hexagonal-encircle ring pattern. According to the reports of metal-assist chemical wet-etching [16], many researchers have mixed etchant to etch selectively the zones which were beneath the silver location via the redox reaction. So, this study used the etchant (BOE and H_2O_2) to etch the structure of Fig. 5(a) and a dot-hollow DWE structure was obtained, as shown

in Fig. 5(b). After DWE, the Ag nanoparticles sunk and the depth was at 10–25 nm.

After dry-etching, the Ag/Si nanostructure with the Ag film on top surface only induced electrons moving from the bottom Si matrix to pass through the Ag film to the top of Ag film [16]. In other words, the electron hole pair would separately locate on the top and the bottom of the Ag thin film. The hole would attract oxyions in the Si surface under the Ag structure, and caused the oxide to sink following the etching in mixed etchant [16]. It is clear that increasing the duration of wet-etching was able to increase the depth of the Ag structures. Notably, when the shape of the Ag structure had changed from particle-like to disk-like, the sink reaction was subject to a new mechanism.

3.4. Ag film and structures of DWE

After ion dry-etching, the shape of the Ag nanostructures affected the mechanism of wet-etching. In Fig. 5, the sink depth of Ag nanoparticles increased with increasing the duration of wet-etching. However, the Ag nano-disks had a slower redox reaction. For physical properties, the Ag nanostructure with dimensions ϕ 450 nm × 30 nm (after dry and wet etching) was used to investigate the DWE mechanism. The DWE sunken nanostructure formed with a hexagonal-encircle ring pattern in Fig. 6(a) and the cross-section image in Fig. 6(b) showed that the sunken characteristic was not obvious. To understand the reason, the sunken mechanism of ion dry-etching film was compared with the un-etched Ag film after wet-etching (Fig. 7). The result showed that the Ag film without dry-etching could attract more electrons to cause a deeper structure than the area with ion dry-etching. Figs. 6 and 7 show that the Si sidewalls were found in the DWE structures. It is important that the sidewall phases not only slowed the redox reaction but also reduced the sink depth of the nanostructure. Notably, the shape of the Ag nanostructures determined the effect of sidewall phases during the DWE process.

Two DWE nanostructures with different Ag nanoshape deposition and cross-section structures are shown in Fig. 8. Region I is the microporous Si sidewalls via wet-etching and it will broaden with increasing the area of the Ag films. This means that region I in the nano-disk case is bigger than that in the nano-particle. In addition, the sink depth of the nano-particle is deeper than that of the nano-disk. One thing, however, is certain: when the size of the nanoparticle was less than 10 nm, this was unable to perform the DWE process.

Moreover, we found that region II (AgGa = Ag + Ga, dry-etching) won't join the redox reaction to sink inside Si matrix. This must be one reason that the Ga doped Ag had changed its oxidative potential to restrain the redox reaction. Due to the Ag_{Ga} layer possessing a passive effect, the Ag nano-disks were hold up by the Si sidewalls during the sinking process. Also, 15–30 nm nano-particles were able to enhance the DWE mechanism in Ag/Si nanostructures. It is for this reason that the sink depth of nano-particles is deeper than that of the nano-disks.

4. Conclusion

By the selective ion etching of FIB, discrete Ag/Si nanorods possessed a multilayer structure and the sidewalls obtained more etching energy and were obviously affected by Ga ion doping. During the DWE process, the Ag_{Ga} layer was able to restrain the wet-etching behavior, and the shape of sidewall phases not only slowed the redox reaction but also reduced the sink depth of the nanostructure. In addition, DWE process was unable to occur on Ag nano-particles of size less than 10 nm. It is believed that adjustment of Ga^+ can fabricate different thickness of tube sidewall for further applications.

Acknowledgements

The authors are grateful to National Cheng Kung University, the Center for Micro/Nano Science and Technology (NCKU Project of Promoting Academic Excellence & Developing World Class Research Center: D98-2700) and NSC 99-2622-E-006-132 for the financial support.

References

[1] S. Miyamoto, K. Nishiguchi, Y. Ono, K.M. Itoh, A. Fujiwara, Appl. Phys. Lett. 93 (2008) 222103.
[2] A. Gruneis, M.J. Esplandiu, D. Garcia-Sanchez, A. Bachtold, Nano Lett. 7 (2007) 3766.
[3] L.A. Ma, T.L. Guo, Mater. Lett. 63 (2009) 295.
[4] M.S. Wang, Q. Chen, L.M. Peng, Small 4 (2008) 1907.
[5] M. Abe, K. Murata1, T. Ataka, K. Matsumoto, Nanotechnology 19 (2008) 045505.
[6] A.M. Morales, C.M. Lieber, Science 279 (1998) 208.
[7] J. Westwater, D.P. Gosain, S. Tomiya, S. Usui, H. Ruda, J. Vac. Sci. Technol. B 15 (1997) 554.
[8] N. Wang, Y.F. Zhang, Y.H. Tang, C.S. Lee, S.T. Lee, Appl. Phys. Lett. 73 (1998) 3902.
[9] S.T. Lee, N. Wang, Y.F. Zhang, Y.H. Tang, MRS Bull. 24 (1999) 36.
[10] R. Juhasz, N. Elfstrom, J. Linnros, Nano Lett. 5 (2005) 275.
[11] F. Hideo, M. Takashi, K. Seigo, Y. Hiroshi, L. Junji, Appl. Phys. Lett. 78 (2001) 2560.
[12] C. Chartier, S. Bastide, C. Lévy-Clément, Electrochim. Acta 53 (2008) 5509.
[13] H. Fang, Y. Wu, J. Zhao, J. Zhu, Nanotechnology 17 (2006) 3768.
[14] B. Fuhrmann, H.S. Leipner, H.R. Hoche, L. Schubert, P. Werner, U. Go1sele, Nano Lett. 5 (2005) 2524.
[15] K. Peng, M. Zhang, A. Lu, N.B. Wong, R. Zhang, S.T. Lee, Appl. Phys. Lett 90 (2007) 163123–163131.
[16] C. Mu, Y. Yu, W. Liao, X. Zhao, D. Xu, X. Chen, D. Yu, Appl. Phys. Lett. 87 (2007) 113104–113111.
[17] X. Qian, J. Li, D. Wasserman, W.D. Goodhue, Appl. Phys. Lett. 93 (2008) 231907.
[18] W. Li, J.Z. Zhou, X. Zhang, J. Xu, L. Xu, W. Zhao, P. Sun, F. Song, J. Wan, K. Chen, Nanotechnology 19 (2008) 135308.
[19] Z.S. Hu, F.Y. Hung, S.J. Chang, K.J. Chen, Y.Z. Chen, Intermetallics 18 (2010) 1428.
[20] A.A. Tseng, Small 1 (2005) 924.
[21] A.A. Tseng, J. Micromech. Microeng. 14 (2004) R15.